Open access • Journal Article • DOI:10.1088/1361-6463/AABC49

Thin films of Ag–Au nanoparticles dispersed in TiO2: influence of composition and microstructure on the LSPR and SERS responses — Source link

Joel Nuno Pinto Borges, Catarina Gonçalves Ferreira, João P. C. Fernandes, Marcos Rodrigues ...+6 more authors

Institutions: University of Minho, University of Lyon, Instituto Superior Técnico

Published on: 25 Apr 2018 - Journal of Physics D (IOP Publishing)

Topics: Surface plasmon resonance and Surface-enhanced Raman spectroscopy

Thin films of Ag-Au nanoparticles dispersed in TiO_2: Influence of composition and microstructure on the LSPR and SERS responses

Joel Borges[1,a)], Catarina G. Ferreira[1,a)], João P.C. Fernandes[1], Marco S. Rodrigues[1], Manuela Proença[1], Mihai Apreutesei[2], Eduardo Alves[3], Nuno P. Barradas[4], Cacilda Moura[1], Filipe Vaz[1]

[1]*Centro de Física, Universidade do Minho, Campus de Gualtar, 4710 - 057 Braga, Portugal*

[2]*Université de Lyon, INSA-Lyon, MATEIS UMR CNRS 5510, 7 Avenue Jean Capelle, 69621 Villeurbanne Cedex, France*

[3]*Instituto de Plasmas e Fusão Nuclear, Campus Tecnológico e Nuclear, Instituto Superior Técnico, Universidade de Lisboa, E.N. 10 (km 139,7), 2695-066 Bobadela LRS, Portugal*

[4]*Centro de Ciências e Tecnologias Nucleares, Instituto Superior Técnico, Universidade de Lisboa, E.N. 10 (km 139,7), 2695-066 Bobadela LRS, Portugal*

[a)] *The first two authors contributed equally to this work*

Corresponding author: Joel Borges. *E-mail:* joelborges@fisica.uminho.pt

Abstract

Thin films containing monometallic (Ag,Au) and bimetallic (Ag-Au) noble nanoparticles were dispersed in TiO_2, using reactive magnetron sputtering and post-deposition thermal annealing. The influence of metal concentration and thermal annealing in the (micro)structural evolution of the films was studied, and its correlation with the Localized Surface Plasmon Resonance (LSPR) and Surface Enhanced Raman Spectroscopy (SERS) behaviours was evaluated. The Ag/TiO_2 films presented columnar to granular microstructures, developing Ag clusters at the surface for higher annealing temperatures. In some cases, the films presented dendrite-type fractal geometry, which led to an almost flat broadband optical response. The Au/TiO_2 system revealed denser microstructures, with Au nanoparticles dispersed in the matrix, whose size increased with annealing temperature. This microstructure led to the appearance of LSPR bands, although some Au segregation to the surface hindered this effect for higher concentrations. The structural results of the $Ag\text{-}Au/TiO_2$ system suggested the formation of bimetallic Ag-Au nanoparticles, which presence was supported by the appearance of a single narrow LSPR band. In addition, the Raman spectra of Rhodamine-6G demonstrated the viability of these systems for SERS applications, with some indication that the Ag/TiO_2 system might be preferential, contrasting to the notorious behaviour of the bimetallic system in terms of LSPR response.

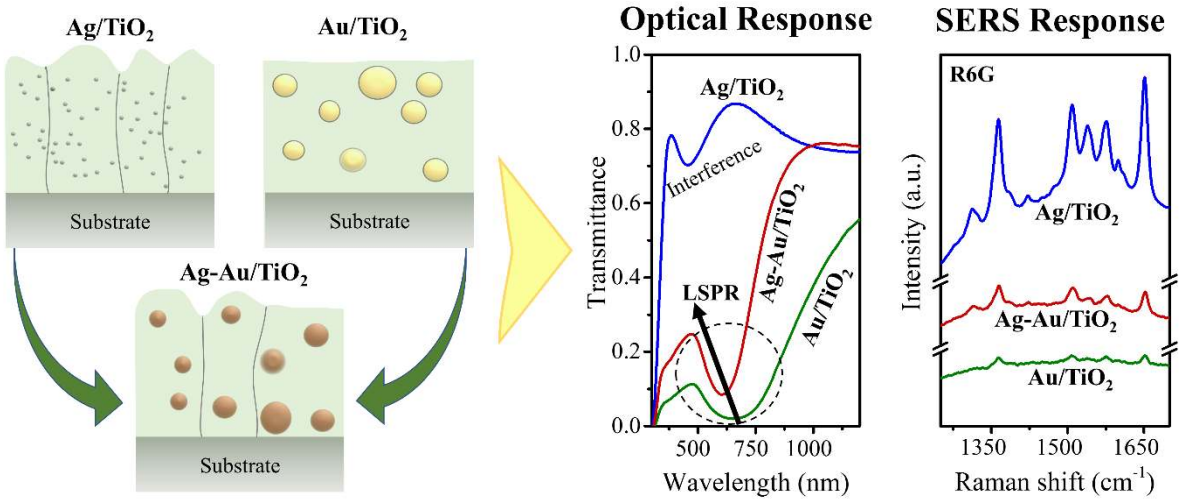

Keywords: Thin Films; Ag-Au Nanoparticles; TiO_2; Localized surface plasmon resonance (LSPR), Surface enhanced Raman spectroscopy (SERS).

1. Introduction

When materials are tailored at the nanoscale, as the case of those containing nanoparticles (NPs), their physical and chemical properties may differ significantly from those of the corresponding bulk materials. In particular, some noble metal NPs exhibit strong absorption bands in the visible, near-infrared or near-ultraviolet regions of the electromagnetic spectrum, associated to the localized surface plasmon resonance (LSPR) phenomenon [1,2]. Surface plasmons (SPs) are collective electronic excitations that occur at a metal-dielectric interface and are accompanied by an oscillating electromagnetic field. They can propagate along the surface of the conductor, being designated by surface plasmon polaritons (SPPs), or be confined to a metallic nanoparticle or nanostructure, in which case are mentioned as localized surface plasmons (LSPs) [3,4].

LSPR leads to the appearance of strong absorption bands, the enhancement of the electromagnetic (EM) field near the nanoparticles and the appearance of scattering to the far field [1,5]. Beyond some known decorative applications [6,7], plasmonic effects are important in a wide range of technological domains, which include plasmon-based photodetectors [8] and modulators [9], gas sensors [10–12], biosensors [13–15], photothermal therapy [16], photodynamic therapy [17], LSP-enhanced solar cells [18,19], surface enhanced Raman spectroscopy (SERS) [20–22], plasmonic nanoscopy [23], thermal emitters [24], light-emitting diodes [25] and magnetic storage [26].

The two most well studied plasmonic metals are gold (Au) and silver (Ag), which exhibit LSPR bands in the visible range of the electromagnetic spectrum [27,28]. While Au has the advantage of being chemically inert and biocompatible, Ag exhibits the sharpest and strongest LSPR absorption among all metals [3,28]. On the other hand, bimetallic Ag-Au nanoparticles are attracting increasing attention due to their improved electronic, optical and catalytic properties [29,30]. According to the preparation method, bimetallic nanoparticles with core/shell or alloyed (where the two constituent metals are mixed at the atomic level) structures may be obtained [31]. In the latter case, the continuous tunability of the LSPR absorption band position between the two single metals may be achievable, by varying the Au/Ag atomic ratio [32]. Since both materials crystalize in face centered cubic (fcc) structures

with very similar lattice constants (407.00 pm for Au and 408.55 pm for Ag), it is possible, in principle, to produce bimetallic Ag-Au nanoparticles of any composition and, consequently, adjust the position of its LSPR band towards a targeted application [27,30].

Due to the unique properties of plasmonic NPs, the preparation of nanocomposite thin films where they are randomly dispersed in a dielectric matrix is becoming an increasingly important subject in the fields of materials science, nanoscience and nanotechnology. In such films, the optical response, and particularly the LSPR band properties are strongly dependent on the nature, size, shape and interparticle spacing of the NPs, as well as on the dielectric properties of the surrounding medium [1,5,7]. To produce these nanocomposite films, Physical Vapor Deposition (PVD) techniques have been frequently used. Magnetron sputtering is an example, and its versatility allows to tailor the chemical and (micro)structural properties of these nanocomposite films towards the above mentioned applications [4]. Nevertheless, when using this method to prepare plasmonic thin films, a second step may be required, especially in the case of low preparation temperatures [5,33,34]. For this purpose, a post-deposition in-air or in-vacuum thermal annealing treatment is often used.

Beyond the work developed by F. Vaz *et al.* [4,35,36], few studies addressed the synthesis of Ag/TiO_2 [37,38] and Au/TiO_2 [39,40] thin films by magnetron sputtering followed by a heat treatment, as an efficient and versatile way to control the morphology, particle growth and optical properties of these nanocomposites. Therefore, the application of this method to prepare bimetallic Ag-Au nanoparticles on a TiO_2 matrix, seems to be a very promising way to achieve different Ag/Au atomic ratios in a dielectric matrix such as TiO_2, which, in principle, will allow to tune the LSPR peak position between those of the corresponding monometallic counterparts.

In the present work, nanocomposite thin films containing monometallic (Ag/TiO_2, Au/TiO_2) and bimetallic (Ag-Au/TiO_2) noble nanoparticles were prepared, with different metal concentrations, in a TiO_2 matrix. A post-deposition annealing treatment was performed in air atmosphere at different temperatures to promote the growth of the metallic nanoparticles with different sizes and distributions, aiming the tuning of their LSPR behaviour. The applicability of some representative

samples of each set to SERS was also accessed in this work, through the enhancement of the Raman signal of a Rhodamine 6G (R6G) solution.

2. Material and methods

Nanocomposite thin films containing single (Ag/TiO_2 and Au/TiO_2) and bimetallic ($Ag\text{-}Au/TiO_2$) noble metal nanoparticles, containing different metal concentrations, were prepared by reactive DC magnetron sputtering, using the sputtering system described in [41,42]. The thin films were deposited on (100) oriented Si wafers (for chemical, structural and morphological characterization), glass lamellae - ISO 8037 and fused silica (SiO_2, to analyze the optical response and the SERS activity) substrates. To obtain the different noble metal concentrations (Ag and/or Au), a rectangular Ti target ($200\times100\times6$ mm^3, 99.8% purity), containing various amounts of gold or/and silver pellets (each one with an area of about 16 mm^2 and 1 mm thick) placed on its preferential erosion zone, were used. The total area of pellets is listed in Table 1.

The target was sputtered in a gas atmosphere composed of Ar (partial pressure of 4.0×10^{-1} Pa) and O_2 (partial pressure of 5.6×10^{-2} Pa, chosen according to the hysteresis experiment [3]), maintaining a constant work pressure of 4.5×10^{-1} Pa during 2 h of deposition. The base pressure of the system was around 4×10^{-4} Pa. The power supply was set to operate in a current regulating mode, using a constant current density of 100 $A\cdot m^{-2}$ applied to the target. A grounded rotating substrate holder was used, positioned 70 mm away from the target, with a constant rotation speed of 9 rpm. No external heating was used during the process. The target potential was measured in each deposition and the values, presented in Table 1, remained roughly constant with the increase of the total area of pellets, showing that the incorporation of silver/gold pellets on the target had no significant influence in the plasma.

Table 1 *Total area of metallic pellets, and cathode (target) potential, for each deposition of the Ag/TiO_2, Au/TiO_2 and Ag-Au/TiO_2 thin films system.*

System	**Ag/TiO_2**			**Au/TiO_2**			**Ag-Au/TiO_2**		
Silver pellets (mm^2)	16	32	48	---	---	---	8	16	24
Gold pellets (mm^2)	---	---	---	16	32	48	8	16	24
Target Potential (-V)	378±3	406±1	404±1	380±2	382±2	382±2	382±2	377±1	378±1

Before the depositions, the substrates were submitted to a plasma activation/etching process to improve the surface cleaning and the adhesion of the thin films. The etching was performed on a Diener low pressure plasma equipment (type Zepto, base pressure of 20 Pa) during 15 minutes in an Ar atmosphere (~90 Pa).

After the depositions, the films were subjected to an in-air heat-treatment protocol to promote the growth of the plasmonic NPs, aiming the tailoring of their structural and morphological features to obtain LSPR and SERS responses. These annealing experiments were conducted in a furnace at atmospheric pressure, using a temperature range varying from 200 °C to 700 °C. A heating ramp of 5°C/min was used, followed by an isothermal period of 1 h at the selected temperature. The samples were then allowed to cool down freely until they reach the room temperature.

The chemical composition of the films was accessed by Rutherford Backscattering Spectrometry (RBS), performed with the IST Van de Graaff accelerator, using 2 MeV $^4He^+$ and 2.3 MeV $^1H^+$ beams, at an angle of incidence of 0º (normal incidence). Three detectors were used, one placed at a 140° scattering angle, and two pin-diode detectors located symmetrical to each other, both at a 165° scattering angle. The RBS profiles were analyzed with the DataFurnace software [43].

Scanning Electron Microscopy (SEM) was used for morphology analysis, performed in a NOVA 200 NanoSEM equipment from FEI, operating at 15 keV. SEM micrographs were also used to calculate the deposition (growth) rate, calculated as the ratio between the average thickness and deposition time.

The evolution of the crystalline structure was studied by X-ray diffraction (XRD) in grazing incidence configuration, with an incident angle of 2º and a step size of 0.04º, using a Brucker D8 Advance System diffractometer, equipped with a Cu-Kα radiation source. The obtained XRD patterns were compared with the Crystallographic Open Database (COD), in order to identify the main phases present in the films. The COD cards used were: Ag (COD-1100136), Au (COD-1100138), Ag-Au (COD-1509205), Anatase-TiO_2 (COD-9008213) and Rutile-TiO_2 (COD-9004141). The peak position and intensity of the Ag and/or Au XRD patterns were fitted using Pearson-VII functions, using a free software (Winfit). The average size of the crystalline domains was also accessed from the integral breadth method (using the fitting results).

The optical transmittance and reflectance spectra of the films were measured using a Shimadzu UV-3101 PC UV−Vis−NIR, equipped with an attached integrating sphere of 60 mm inner diameter. To eliminate the experimental artefacts caused by the integrating sphere and thus to correct the reflectance spectra, two standards were used: a STAN-SSH High-Reflectivity specular reflectance standard and a WS-1-SL Spectralon white reflectance standard.

For surface enhanced Raman spectroscopy measurements, the samples were immersed during 7 hours in a 10^{-4} M solution of Rhodamine 6G in ethanol, and then dried in air for one day. The SERS measurements were performed at room temperature with Horiba Jobin Yvon T64000 triple Raman spectrometer, equipped with a liquid nitrogen cooled charge couple device (CCD) Symphony II 1024×246 FIVS detector, with a resolution better than 1 cm^{-1}. The excitation line, 514.5 nm, of an argon ion laser was focused onto the sample using a ×50 MS Plan objective of an Olympus Microscope BHSM, in a back-scattering geometry. The spectra were obtained with a measured power of about 0.4 mW on the sample, during an integration time of 30 s, with 5 accumulated scans.

3. Results and Discussion

3.1. Characteristics of growth and composition of the as-deposited films

The morphology and deposition rate of the as-deposited films are shown in Figure 1. Regarding the monometallic nanocomposite thin films, the Ag/TiO_2 system shows the development of a porous and low compact columnar microstructure (lowest pellets area), which evolves to a granular voided growth with the increase of silver pellets area, associated to a porous and disordered structure and an extremely rough surface (clearly observed by the micrograph of the sample deposited with pellets area of 48 mm^2). This can be attributed to the increase of the amount of Ag atoms reaching the film during the early stages of its growth, as also previously reported and discussed in other related works [34,44]. On the other hand, the Au/TiO_2 system presents a dense and compact morphology, with very low surface roughness, regardless the gold pellets area, once again in accordance with some previous results [3,44].

When both noble metals are present in the films (bimetallic Ag-Au/TiO_2 system), the morphology is characterized by dense regions, together with granular microstructures, although the distribution of these structures in the samples varied according to the pellets area. Based on the SEM micrographs of the systems with a single noble metal, Ag/TiO_2 and Au/TiO_2 (Figures 1a, 1b), this kind of morphologies may indicate the existence of a phase separation between Au and Ag, with the appearance of Au-rich and Ag-rich regions in the as-deposited thin films. When the total area of pellets is lower, dense columnar microstructures are predominant (similar to the ones present in the Au/TiO_2 films), even though it is possible to observe the presence of few granular microstructures at the surface, which might be regions where Ag is agglomerating with more prevalence. Increasing the silver and gold pellets in the target led to the formation of "hybrid" films, composed by dense regions and granular microstructures, where the former are most probably regions where Au is prevailing and the latter corresponding to Ag agglomeration zones. For the highest content of silver and gold pellets, the film obtained is mainly constituted by porous granular structures, although these are denser than the ones observed for the Ag/TiO_2 samples. Moreover, and regarding the surface of this set of samples, it seems that the surface roughness also increased with the total area of pellets, a trend that is similar to Ag/TiO_2 films.

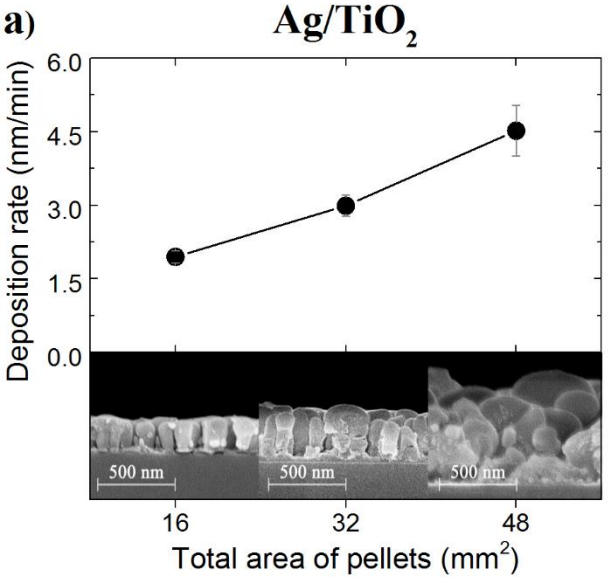
a)
Ag/TiO2
Deposition rate (nm/min)
6.0
4.5
3.0
1.5
0.0
500 nm
500 nm
500 nm
16
32
48
Total area of pellets (mm2)

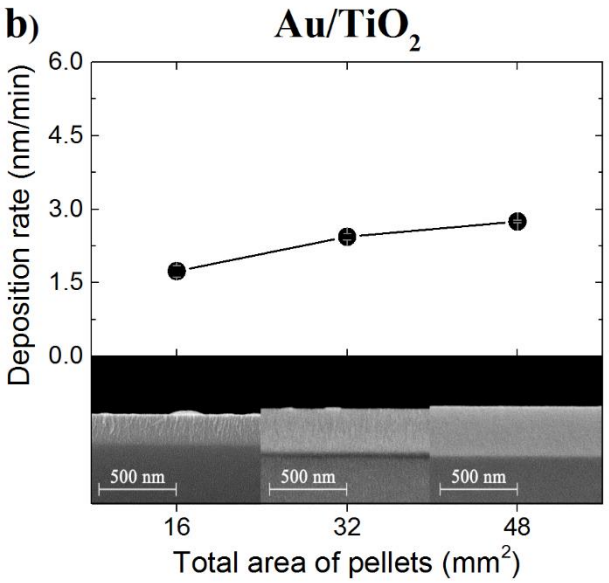
b)
Au/TiO2
Deposition rate (nm/min)
6.0
4.5
3.0
1.5
0.0
500 nm
500 nm
500 nm
16
32
48
Total area of pellets (mm2)

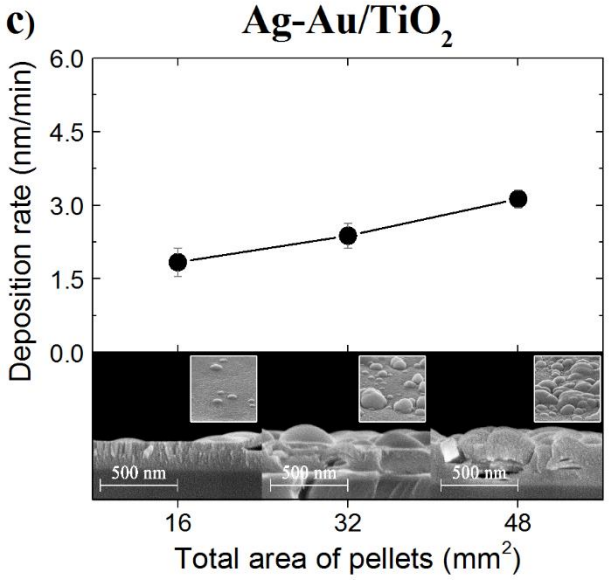
c)
Ag-Au/TiO2
Deposition rate (nm/min)
6.0
4.5
3.0
1.5
0.0
500 nm
500 nm
500 nm
16
32
48
Total area of pellets (mm2)

Figure 1 *Cross-sectional SEM micrographs and deposition rate of the as-deposited films as a function of the total area of pellets incorporated in the Ti target for the monometallic, (a) Ag/TiO_2 and (b) Au/TiO_2, and bimetallic (c) Ag-Au/TiO_2 nanocomposite thin films. SEM micrographs of the surfaces of the Ag-Au/TiO_2 thin films are also presented in (c).*

The deposition (growth) rate had an expected increased with the content of silver and/or gold pellets on the target, for all sets of samples. The behaviour of the deposition rate is directly related to the larger sputtering yields of Ag and Au comparatively to TiO_2 [45,46]. This leads to a significant increase of the flux of Ag and/or Au atoms sputtered from the target when the pellets' area increases, while the flux of Ti atoms remains approximately the same. Such an increase is particularly notorious for the Ag/TiO_2 films, where a change in the pellets area, from 16 mm^2 to 48 mm^2, was followed by an increase in the deposition rate from 2.0 nm/min to 4.5 nm/min. For the Au/TiO_2 samples, the variation of the deposition rate was quite smooth, assuming values in the range from 1.7 nm/min to 2.8 nm/min. The sharpest growth of the deposition rate observed for the Ag/TiO_2 films relatively to Au/TiO_2 cannot only be attributed to the higher sputtering yield of Ag in comparison to Au [47,48], but also to morphological changes. Since the films with higher contents of Ag are more porous, and thus have a lower density, the deposition rates (or, more precisely, the growth rates) measured for the Ag/TiO_2 samples are influenced by this change of morphology. In contrast, the Au/TiO_2 films, that possess denser microstructures are the ones presenting the lowest deposition rates.

For the bimetallic nanocomposite system, Ag-Au/TiO_2, the same increase in the pellets area (from 16 mm^2 to 48 mm^2) led to an increment of the deposition rate from 1.8 nm/min to 3.1 nm/min. The trend observed in the deposition rate along with morphological evolution discussed before clearly suggests that the bimetallic system follows an intermediate behaviour between the two monometallic nanocomposite systems.

The results from RBS analysis, performed to the as-deposited samples, revealed that the atomic ratio C_O/C_{Ti} was approximately 2 for all the samples studied, which suggests the formation of close-stoichiometric TiO_2 matrices. As expected, the atomic percentage (at.%) of Ag and Au in the films is

expectedly correlated with the total area of pellets incorporated in the Ti target, following the trends displayed in Figure 2.

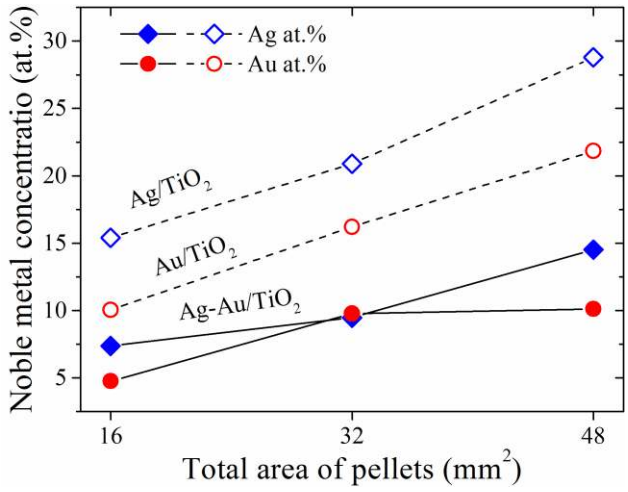

Figure 2 *Atomic concentration of Ag (blue) and Au (red) present in the as-deposited samples, as a function of the pellets area, for the monometallic (Ag/TiO2, Au/TiO2) and bimetallic (Ag-Au/TiO2) nanocomposite thin films.*

An almost linear increase of the metallic content of the films is observed for all systems, denoting that the higher sputtering yields of Au and Ag (comparatively to TiO_2) are controlling the composition evolution process [45,46]. The increase of the total area of silver pellets (Ag/TiO_2 system) from 16 mm^2 to 32 mm^2 and to 48 mm^2 resulted in a growth of the atomic concentration of Ag in the films, from 15.4 at.% to 20.9 at.% and then to 28.8 at.%. Although shifted to lower values, a similar trend was observed for the Au/TiO_2 thin films, where Au contents of 10.0 at.%, 16.2 at.% and 21.8 at.% were obtained. This means that the concentration of Au is about two thirds lower than that of Ag, for the same pellets area. The higher sputtering yield of Ag, in comparison to Au [47,48], led to an increase of the metal flux sputtered from the target, for the same pellets area. This explains the differences observed between the two monometallic nanocomposite systems.

Regarding the bimetallic nanocomposite ($Ag-Au/TiO_2$) system, atomic concentrations of Ag and Au of 7.4 at.% and 4.8 at.%, respectively, were measured for a total area of pellets of 16 mm^2. Since the

concentration of each metal in this sample is not very high, it is not surprising that only few granular microstructures appeared on the surface, due to the presence of silver (see Figure 1c). When the total area of pellets is 32 mm^2, the content of Ag increases to 9.5 at.% while the atomic concentration of Au more than duplicates, reaching the value 9.8 at.%. The presence of similar contents of Ag and Au in this sample is in agreement with the "hybrid" morphology of these films, previously observed in the SEM micrographs, Figure 1. On the other hand, when the total area of pellets in the target is 48 mm^2, the resultant as-deposited film has an atomic concentration of Ag of 14.5 at.% and an Au content of 10.1 at.%. Morphologically, this sample is mainly composed by porous granular structures, which may probably be related with the prevalence of silver in the film. From now on, the films will be mentioned according to their at.% of Ag and Au.

3.2. Morphological and crystalline evolution with annealing treatments

Detailed characterization of the morphological and crystalline changes operated in the thin films during the thermal treatment were carried out to further understand the evolution of the bimetallic Ag-Au/TiO_2 system, always taking as reference the behaviour observed in the monometallic nanocomposite systems (Ag/TiO_2 and Au/TiO_2).

SEM micrographs, taken in cross-section and tilted angles, to observe the surface of the films, and XRD patterns to study the structural evolution of the films with annealing treatments, are displayed in Figure 3 and Figure 4. Only the films with the lowest atomic concentrations of Ag and/or Au are presented (i.e. the ones sputtered from a target with a total area of pellets of 16 mm^2), since they were found to be representative of the most important changes observed between systems, in what concerns the structural and morphological features.

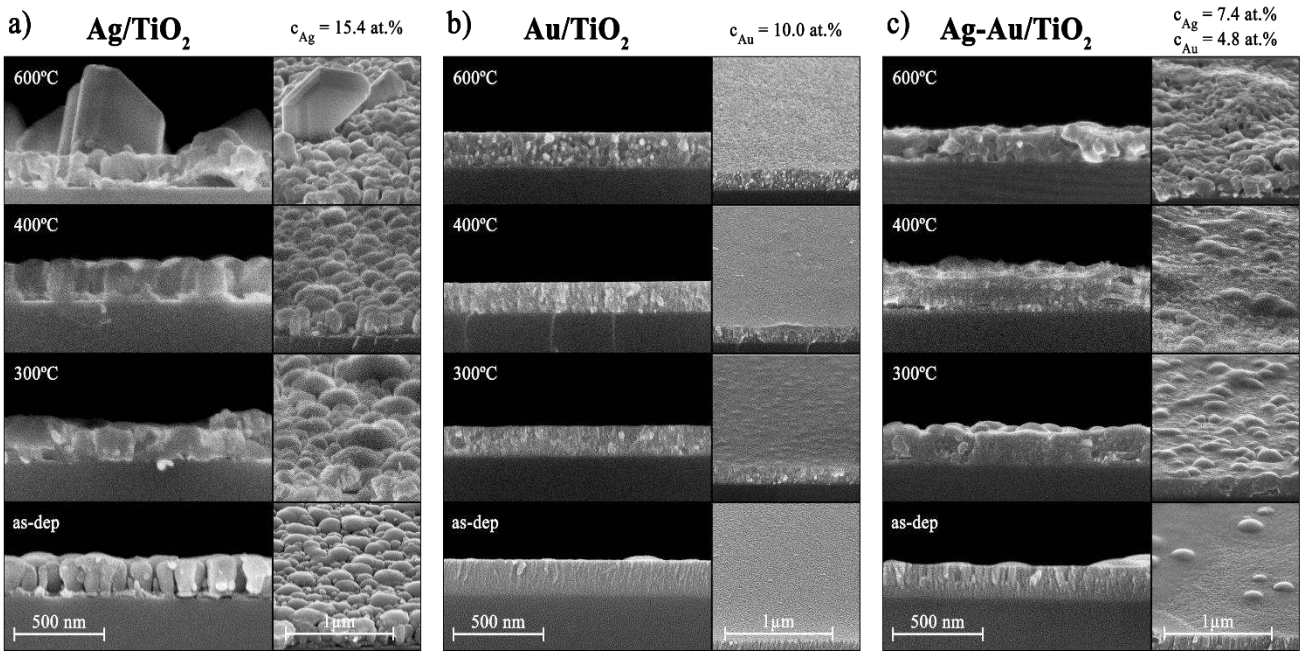

Figure 3 *SEM micrographs observed in cross-section (left) and tilted angles (right) of the (a) Ag/TiO2, (b) Au/TiO2 and (c) Ag-Au/TiO2 thin films systems, deposited with the lowest number of silver and gold pellets (total area of 16 mm^2), for different annealing temperatures.*

The monometallic system composed by Ag (15.4 at%) dispersed in TiO_2 shows two major morphological changes when the samples are subjected to thermal annealing at different temperatures. The as-deposited film presents a porous columnar microstructure (Figure 3a). With the increase of the annealing temperature, these columnar microstructures seem to disappear, and a more disordered, and granular, morphology is obtained. Furthermore, the heat-treatment speeds up the diffusion processes, promoting the aggregation of Ag clusters into larger crystalline domains, as previously reported for this kind of systems [34]. After annealing at 600 °C, the diffusion of Ag is promoted along their grain boundaries towards the surface. As a result of this diffusion process, the formation of large polyhedral-shaped Ag crystallites was observed on the surface of the films.

In contrast to the previous analysis, the other monometallic system, Au/TiO_2 (10.0 at.% Au), did not experienced major changes in their morphological features, even though the annealing treatment have influenced the growth and diffusion of the Au nanoparticles. It presents a typical dense and compact morphology, although the as-deposited sample reveals compact columnar microstructures that are no longer distinguishable after the heat-treatment. The formation of Au nanoparticles is then observed

for the films subjected to thermal annealing (bright grains in the SEM micrographs). These nanoparticles grow in size with the increase of the annealing temperature as a result of the thermal energy, promoting their diffusion and coalescence [3,33].

Regarding the bimetallic Ag-Au/TiO_2 system, a clear change in the morphology is observed when the samples are subjected to the thermal annealing process and, once again, it seems that presents morphological characteristics of both monometallic systems combined in a single one. As abovementioned the as-deposited Ag-Au/TiO_2 film presents a dense microstructure, although it is possible to identify the existence of some granular structures on the surface. This suggested the separation between Ag-rich and Au-rich regions throughout the film, being the granular structures attributed to the presence of Ag in the samples, since Au leads to the formation of smoother surfaces (see as-deposited sample in Figure 3). However, the annealing process leads to a progressive change of the morphology of the films and the separation between dense and granular regions is no longer perceptible. This behavior might suggest that the heat-induced diffusion of the Ag and Au atoms throughout the matrix is probably resulting in the formation of bimetallic alloy Ag-Au nanoparticles, which agrees with what was reported for similar films deposited on SiO_2 [49]. Anyway, it is important to emphasize that, based only in SEM analysis, the formation of separated phases of Ag and Au cannot be disregarded at the time. To further evaluate which crystalline phases are present in the films, a detailed XRD analysis was performed as a function of the annealing temperature. The diffractograms obtained for the monometallic, Ag/TiO_2 and Au/TiO_2, and bimetallic Ag-Au/TiO_2 nanocomposite films are plotted in Figure 4.

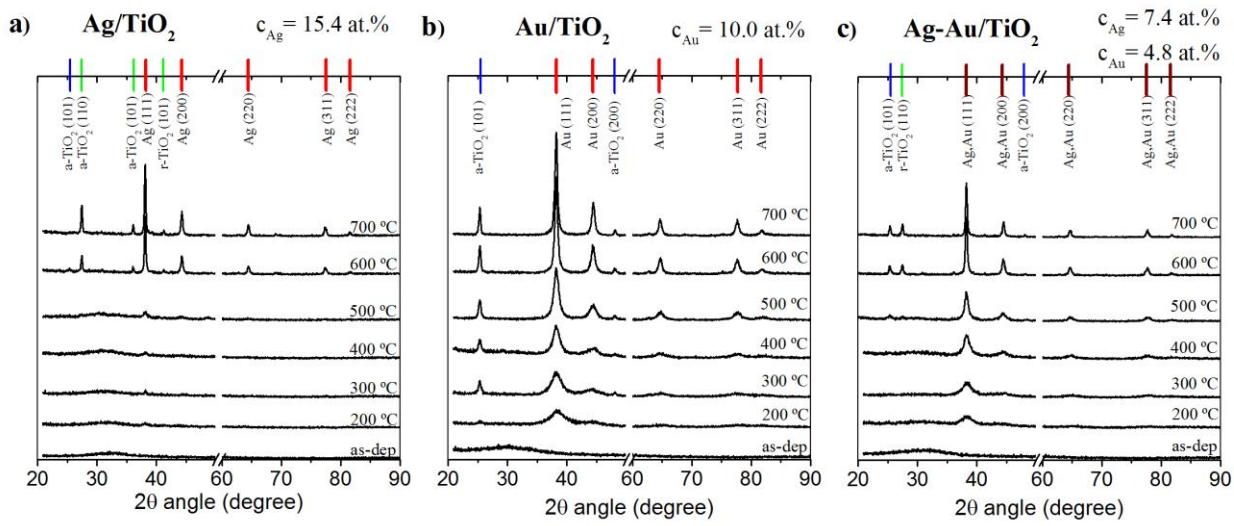

Figure 4 *XRD diffractograms of the (a) Ag/TiO2, (b) Au/TiO2 and (c) Ag-Au/TiO2 films (lowest noble metal content) subjected to different annealing treatments. Each diffractogram is vertically shifted for better visualization.*

Based on XRD results, all as-deposited samples reveal an amorphous structure, regardless their composition. This behavior is characterized only by a broad scattering maximum without any Bragg diffraction peaks. As the annealing temperature was increased, a progressive crystallization of the Ag, Au and TiO_2 phases takes place, whose intensities depend on the concentration of metal in the films.

For the Ag/TiO_2 samples, annealing treatments promoted the crystallization of Ag in its typical face centered cubic (fcc) structure (COD-1100136), characterized by diffraction peaks indexed to the (111), (200), (202), (311) and (222) crystal planes. However, the Ag (111) diffraction peak is the most visible for temperatures in the range 200 ºC - 500 ºC, denoting also a poor crystallization of Ag since their intensities are quite low. Nevertheless, it becomes considerably more pronounced for the highest annealing temperatures (600 ºC and 700 ºC). At the same time, the other Ag crystallographic orientations start to appear in the diffractograms for increasing annealing temperatures. Considering the SEM analysis (see Figure 3), the results may be attributed to the growth of Ag crystals that stay embedded in the TiO_2 matrix for temperatures up to 500 ºC, giving rise to faint diffraction peaks. For

higher temperatures (600 ºC and 700 ºC), the diffraction peaks increase in intensity, becoming narrower, and new orientations appear. This might be an evidence that Ag segregates to the surface of the films, resulting in the formation of large crystalline domains [34,50]. Also important to note is the crystallization of TiO_2, which occurs at higher temperatures (600 and 700 ºC). In these cases, the TiO_2 crystalizes in its rutile phase (COD-9004141), as evidenced by the presence of the r-TiO_2 (110), (101) and (111) diffraction peaks, properly identified in Figure 4a. Furthermore, it is also possible to observe a faint peak, at 600 ºC, indexed to the (101) crystal plane of the anatase phase of TiO_2 (COD-9008213), in addition to the peaks corresponding to its rutile phase.

For the Au/TiO_2 samples, the Au crystallization in its most common structure, fcc (COD-1100138), started for an annealing temperature of 200 ºC. At this temperature, only a broad diffraction peak corresponding to the Au (111) crystal plane is observed. With the increase of the annealing temperature, this peak becomes sharper and more intense. A new set of diffraction peaks indexed to the (200), (202), (311) and (222) crystal planes of the Au, appears at 400 ºC and its intensity also increases with the temperature, indicating a progressive crystallization of the Au phase. It is also important to mention that the Au XRD peaks become particularly pronounced for the samples with intermediate (16.2 at.%) and higher (21.8 at.%) contents of Au, and subjected to heat-treatments between 400 ºC and 700 ºC (diffractograms not showed). This behavior is most probably related with the segregation and formation of Au clusters on the surface of the films, as already observed in a previous study [3]. Regarding the TiO_2 matrix containing Au, a crystallization in its anatase phase was observed for temperatures above 300 ºC, with the appearance of the a-TiO_2 (101) and (200) peaks in the diffractograms. The rutile phase (110) only appears for the intermediate and the highest Au concentrations, and for an annealing temperature of 700 ºC, where both phases coexist (anatase and rutile).

Before starting the analysis of the bimetallic Ag-Au/TiO_2 system, it is worth mentioning that the metallic phases have similar lattice parameters. The values are 408.55 pm for Ag (COD-1100136), 407.00 pm for Au (COD-1100138) and 407.60 pm for Ag-Au (COD-1509205). Therefore, the

diffraction positions of bimetallic Ag-Au phases are very close to the ones of Ag and Au. More precisely, the XRD peaks of Ag-Au phases appear in intermediate positions, between Ag and Au, and with 2θ shifts in the order of a few hundredths of degree, which is comparable to the resolution of the equipment used.

The structural behavior of the Ag-Au/TiO_2 films subjected to heat-treatment is characterized by a broad diffraction peak at an angular position indexed to the (111) orientation, increasing their intensity and becoming progressively sharper with the annealing temperature. Additional diffraction peaks, indexed to the (200), (202), (311) and (222) planes, become noticeable for annealing temperatures from 400 ºC. A careful analysis of the XRD patterns also indicates the existence of single peaks, meaning that only one phase might be present in the films thereby suggesting the formation of crystalline domains of Ag-Au (possibly bimetallic alloy nanoparticles). This claim is also in agreement with similar studies where Ag-Au where deposited in SiO_2 [49].

The lattice parameters were also calculated for the crystalline samples of each system (see Figure 5a) and showed small differences from the corresponding bulk materials. The differences are more pronounced in the Au/TiO_2 system, which showed an average value of about 407.9±0.2 pm (0.9 pm higher than the bulk state), while for Ag/TiO_2 films the average value was estimated in 408.8±0.2 pm (0.3 pm higher than the bulk state). Moreover, for Ag-Au/TiO_2 films the average value of the lattice parameter was estimated in 407.7±0.2 pm, which is even close to the bulk material (407.60 pm). Furthermore, the bimetallic system Ag-Au/TiO_2 follows a trend where the lattice parameter values are always close or beneath Au/TiO_2 system, which by itself are below the Ag/TiO_2 system (see Figure 5a).

In the Ag-Au/TiO_2 system, the crystallization of the TiO_2 matrix starts when the annealing temperature is 500 ºC, but becoming more evident for higher annealing temperatures (600 ºC and 700 ºC). In the latter cases, both anatase and rutile crystalline phases coexist in the host matrix, as evidenced by the presence of the a-TiO_2 (101) and the r-TiO_2 (110) diffraction peaks in the XRD

spectra of these films. These results once again show that the crystalline structure of the bimetallic system follows a behavior that is roughly between those observed in the monometallic systems.

By fitting the XRD peaks of Ag, Au and Ag-Au, it was also possible to estimate the average size of the crystalline domains of metal (Ag, Au, Ag-Au), as a function of the annealing temperature and for all concentrations. The results obtained are illustrated in Figs. 5b for the monometallic (Ag/TiO_2, Au/TiO_2) and bimetallic $Ag\text{-}Au/TiO_2$ nanocomposite systems. In general, the average size of the crystalline domains (grain size) increases with the annealing temperature for all sets of samples, although its evolution seems to follow different tendencies according to the system analyzed.

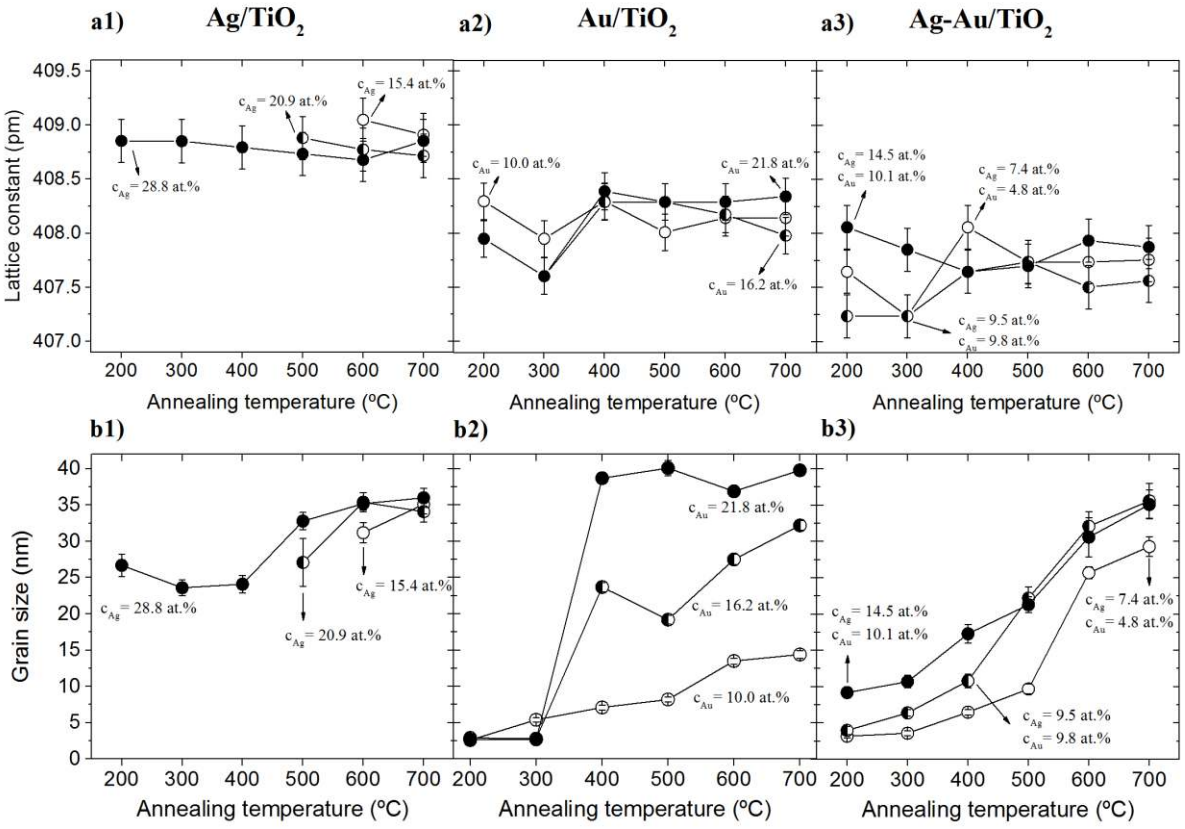

Figure 5 *Estimated* ***a)*** *lattice constants and* ***b)*** *grain size as a function of the annealing temperature for (a1 and b1) Ag/TiO_2, (a2 and b2) Au/TiO_2 and (a3 and b3) $Ag\text{-}Au/TiO_2$ systems with different contents of Ag and/or Au.*

The Ag/TiO_2 films with the lowest (15.4 at.%) and intermediate (20.9 at.%) contents of Ag are poorly crystallized up to about 500 ºC and, therefore, a reliable quantification of the grain size was not

possible below this temperature. For higher temperatures, Ag is segregating to the surface of the films to form large clusters, as shown in SEM micrographs (Figure 3), leading to intense and sharp XRD peaks. The average grain sizes of those films were estimated to be in the range of 30 nm - 35 nm. On the other hand, the Ag/TiO_2 samples with 28.8 at.% of Ag present measurable crystalline domains from 200 ºC, with average sizes of 25 nm and up to 35 nm, when the films are heated at 700 ºC. Therefore, as the Ag content increases, the Ag nanoparticles start to crystallize at lower temperatures. Regarding the Au/TiO_2 films, the increment in the annealing temperature from 200 ºC to 700 ºC induced an almost linear and smooth increase of the average grain size, from nearly 2.5 nm to almost 15 nm, for the samples with the lowest concentration of Au (10.0 at.%). These results are in accordance with the SEM analysis that showed a progressive growth in size of the Au nanoparticles throughout the matrix with the increase of the annealing temperature. For higher Au contents (16.2 at.% and 21.8 at.%) nanoparticles with few nanometers are observed when the films are annealed up to 300 ºC. For 400 ºC and above the grain size sharply increases, approximately one order of magnitude, oscillating between 20 nm and 30 nm for the intermediate composition (16.2 at.%), and reaching about 40 nm for the highest composition (16.2 at.%), Figure 5b). As aforementioned, this behavior might be the result of the segregation of Au to the surface of the films [3].

For the Ag-Au/TiO_2 samples, an increase of the grain size with the temperature was also observed, presenting similar and smoother trends for all compositions. When these films are annealed at 200 ºC or 300 ºC, the size of the metallic nanoparticles is confined to few nanometers, similar to what happened for the Au/TiO_2 samples, which probably indicates that the Ag and Au atoms do not strongly inter-diffuse for heat-treatments up to 300 ºC. After that, the nanoparticles grow quite smoothly for temperatures up to 500 ºC, where grain sizes of about 10 nm were estimated for the film with lowest metal concentration (7.4 at.%, Ag and 4.8 at.%, Au), while the remaining samples present a grain size of approximately 20 nm. This soft increase of the grain size is possibly related with the formation of Ag-Au bimetallic nanoparticles that progressively grow as more gold and silver atoms start to diffuse and to combine, promoted by the thermal annealing. From 500 ºC to 700 ºC, the grain

size increases more substantially, probably due to the segregation, followed by aggregation, of large crystalline structures to the surface, reaching values close to 30 nm for the sample with the lowest metallic content and nearly 35 nm for the films with intermediate and higher concentrations of Ag-Au.

3.3. Optical response

The influence of the annealing temperature on the optical response and LSPR effect of all sets of films was studied via spectrophotometry analysis. The transmittance and reflectance spectra of some representative samples are depicted in Figure 6.

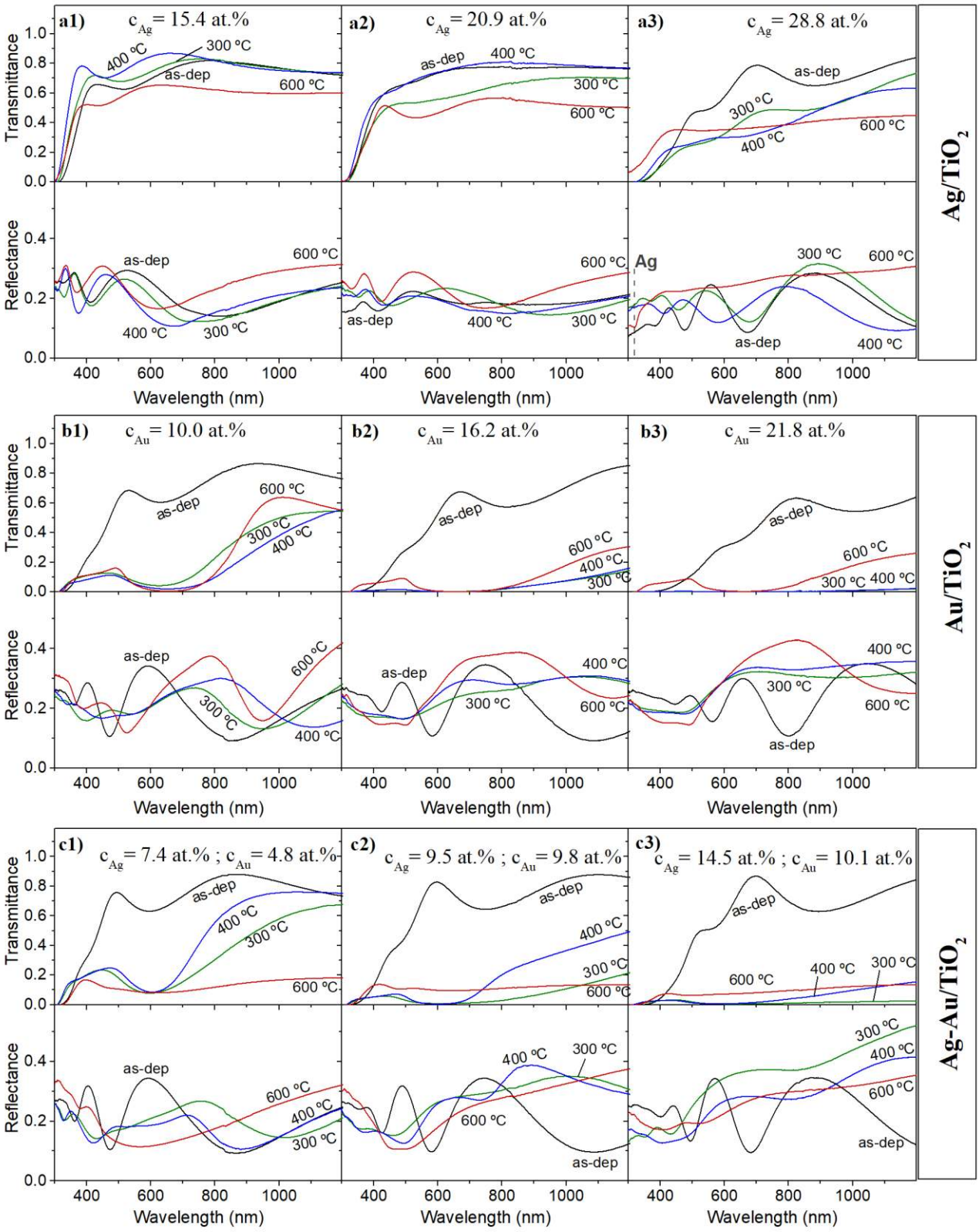

Figure 6 *Transmittance and reflectance spectra of the (a) Ag/TiO_2 (a), (b) Au/TiO_2 (b) and (c) $Ag\text{-}Au/TiO_2$ films with different contents of Ag and/or Au and subjected to different annealing treatments.*

The as-deposited samples of Ag/TiO_2, Au/TiO_2 and $Ag\text{-}Au/TiO_2$ revealed an interference-like behavior, characteristic of semi-transparent thin films (when their thickness is of the same order of magnitude as the incident wavelength [51]). The most important feature of these samples is the presence of interference fringes in their spectra, without any evidence of plasmonic effects due to LSPR, since Ag and/or Au are still homogenously dispersed inside the matrix in the form of low-sized nanoparticles. However, as soon as these films are subjected to heat-treatment, their optical response dramatically changes, as consequence of the formation and growth of monometallic and/or bimetallic noble nanoparticles dispersed inside, or on the top, of the TiO_2 matrix. In fact, according to the XRD and SEM analysis, different microstructures were achieved by varying the composition and temperature of the annealing treatment applied to the films. It is thus expected that different optical responses may arise if the films are nanocomposite materials or if they hold metallic clusters on its surface.

For the Ag/TiO_2 system, the interference profiles continue to be observed when the films undergo thermal annealing up to 600 ºC, for the samples with the lowest and intermediate contents of Ag (Figs. 6.a1 and 6.a2). Moreover, for heat-treatments at 600 ºC, it is also possible to observe a little decrease in the transmittance in the whole spectrum, which might be related with the presence of large silver aggregates at the surface, that hinder the light transmission through the film. When the concentration of Ag is 20.9 at.%, the position of the interference fringes (only clearly distinguishable in the reflectance spectra) remains approximately unchanged with the annealing treatment, even though the intensity of the reflected light seems to slightly enhance for the sample annealed at 600 ºC. This behavior is complemented by a reduction of the transmitted light and is attributed to the segregation of large silver clusters to the surface of the film, which promotes the light scattering, resulting in an increase of the reflectance and in a decrease of transmittance. Regarding the samples with the highest content of Ag (28.8 at.%), Figure 6.a3, the interference fringes are only visible for heat-treatments up to 400 ºC, and the distance between two consecutive maxima/minima decreases with the temperature, probably associated with an increase of the film's thickness [51]. On the other

hand, for the sample subjected to thermal annealing at 600 ºC, the transmittance and reflectance profiles present unusual almost flat profiles ranging from about 450 nm to 1200 nm. This behaviour is attributed to the formation of Ag fractal structures on the top of the TiO_2 matrix after thermal annealing, already reported in a previous work [36] and also observed by A. Biswas et al. [52]. The fractal aggregates incorporate an enormous variety of shapes and spatial scales, which make their spectral optical response very broad and almost featureless. Additionally, a peak located at approximately 320 nm is observed in the reflectance spectrum of the sample (properly indicated in Figure 6.a3)) and corresponds to the signature of the onset of interband transition involving d-electrons in Ag. To further confirm the existence of these Ag fractal aggregates on top of the TiO_2 matrix, surface micrographs of this sample were taken and two examples of dendrite-type fractal structures found in the film are presented in Figure 7.

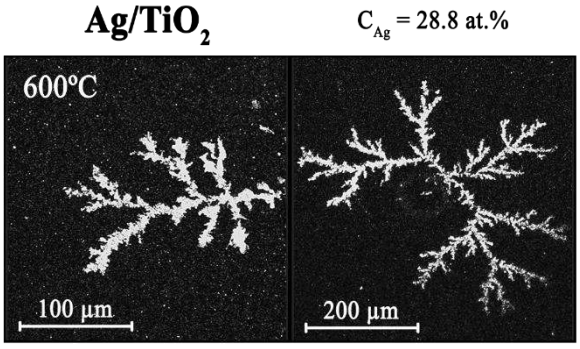

Figure 7 *Surface micrographs of two different Ag fractal structures observed on top of the Ag/TiO_2 film with Ag content of 28.8 at.% and annealed at 600 ºC.*

For the Au/TiO_2 system, the heat-treatment promotes the appearance of strong and large LSPR bands located between 600 nm and 700 nm. The reflectance spectra maintain their interference-like profiles, especially for the samples with the lowest contents of Au, although this behavior is markedly attenuated when the films undergo thermal annealing, especially near the wavelengths where LSPR occurs. Regarding the samples with the lowest concentration (10.0 at.%), Figure 6.b1), the morphological and crystalline modifications induced in the films by thermal annealing led not only to a reduction of the transmittance in the whole spectrum, but also to a broadening of the LSPR band.

This behaviour was previously observed in similar systems and may be attributed to the crystallization and growth of large and well-separated Au nanoparticles inside the TiO_2 matrix during the heat-treatment [5]. In addition, the position of the LSPR peak is red-shifted about 30 nm (from nearly 625 nm to 655 nm) with the increase of the annealing temperature from 300 ºC to 600 ºC, probably due to an increase of the refractive index of host the matrix [4]. This is in agreement with the XRD results (Figure 4) that revealed a progressive crystallization of the TiO_2 matrix into its anatase phase (which refractive index is higher than that of amorphous TiO_2) thereby increasing the wavelength at which the resonance occurs [5]. On the other hand, the samples with intermediate (16.2 at.%) and higher (21.8 at.%) concentrations of Au (Figs. 6.b2 and 6.b3)become completely opaque in the range 600 – 700 nm (i.e. their transmittance values drop to zero) when subjected to heat-treatment at 300 ºC and above, with the appearance of an extremely broad LSPR band in that region. This is attributed to the strong absorption by Au nanoparticles dispersed throughout the matrix. Nevertheless, an additional feature appears in their reflectance spectra, between 350 nm and 500 nm, which is characteristic from bulk-Au [53,54]. These results clearly suggest that Au clusters segregate to the surface of the films, which in fact is in agreement with the microstructural results. This means that two different effects are taking place when these samples undergo thermal treatment, strongly influencing their optical response: i) the formation and growth of well separated Au nanoparticles that remain inside the matrix contributing for LSPR absorptions and ii) the segregation of large Au clusters towards the surface, which are decreasing the transmittance spectrum due to light absorption by this top layer.

Regarding the Ag-Au/TiO_2 films, it was verified that the morphological modifications promoted by the heat-treatment led to a notorious reduction of the transmittance along all spectral range considered and, in some cases, to the appearance of LSPR absorption bands, narrower than those of the Au/TiO_2 system. The interference behavior continued to be observed in the reflectance spectra, although it has been strongly attenuated for the films subjected to thermal annealing. For the samples with the lowest metal concentration (7.4 at.%, Ag and 4.8 at.%, Au), Figure 6.c1), the LSPR band is only clearly visible for heat-treatments at 300 ºC and 400 ºC and is located around 600 nm, blue-shifted in

comparison to the Au/TiO_2 films. For the sample annealed at 600 ºC, the transmittance is very low in the whole spectrum. These results seem to indicate that when the films are annealed at 300 ºC and 400 ºC, there are some diffusion of the Au and Ag atoms throughout the matrix, with the formation of the bimetallic Ag-Au nanoparticles, that push the LSPR peak towards lower wavelengths, when compared to the Au/TiO_2 system. The presence of only one LSPR band confirms by itself the formation of Ag-Au alloy structures [55]. At the same time the LSPR band sharpens, which might be an indication of a lower dispersion in the sizes of the nanoparticles, being important for certain kind of applications (e.g. LSPR-biosensing, where narrow bands are preferable [13,14]). Notwithstanding, for the sample annealed at 600 ºC, a higher number of Ag and Au atoms may have interdiffused to form large Ag-Au bimetallic clusters, as reported in an analogous study [49]. These bimetallic clusters may be predominantly at the top of the film, increasing the scattering of the incident light and resulting in a reduction of the transmittance in the entire spectrum. Considering the films with intermediate concentrations (9.5 at%, Ag and 9.8 at.%, Au) it was observed that the dependence of the optical properties with the annealing temperature followed a very similar trend in respect to the samples with lower metallic contents. However, in this case the LSPR absorption band observed for the films annealed at 300 ºC and 400 ºC is broader, although its minimum is also located around 600 nm. Besides, in the vicinity of the LSPR peak, the transmittance vanishes and thus the films become totally opaque in that region. Finally, for the films with the highest contents of metal (14.5 at.%, Ag and 10.1 at.%, Au), the transmittance is extremely low in the whole spectral range and the LSPR band is very broad and smooth. This behaviour may be attributed to an intense segregation of both metals to the surface, which reduces the amount of light transmitted through the sample. At the same time, the reflectance profiles only show the typical interference fringes with any evidences of other structures such as fractals (observed only in the monometallic nanocomposite system of Ag/TiO_2).

3.4. Application to SERS

The SERS spectra of the R6G molecules adsorbed onto the surface of some representative samples is plotted in Figure 8. For this application, only the films Ag/TiO_2 with 15.4 at.% of Ag, Au/TiO_2 with 10.0 at.% of Au and Ag-Au/TiO_2 with 14.5 and 10.1 at.% of Ag and Au, respectively, were used since they were the sets of films that showed the most relevant SERS signals. The spectra of the R6G directly deposited on the substrates are not shown in this work, since the Raman signal collected in this case is negligible, without any trace of the characteristic peaks of the rhodamine.

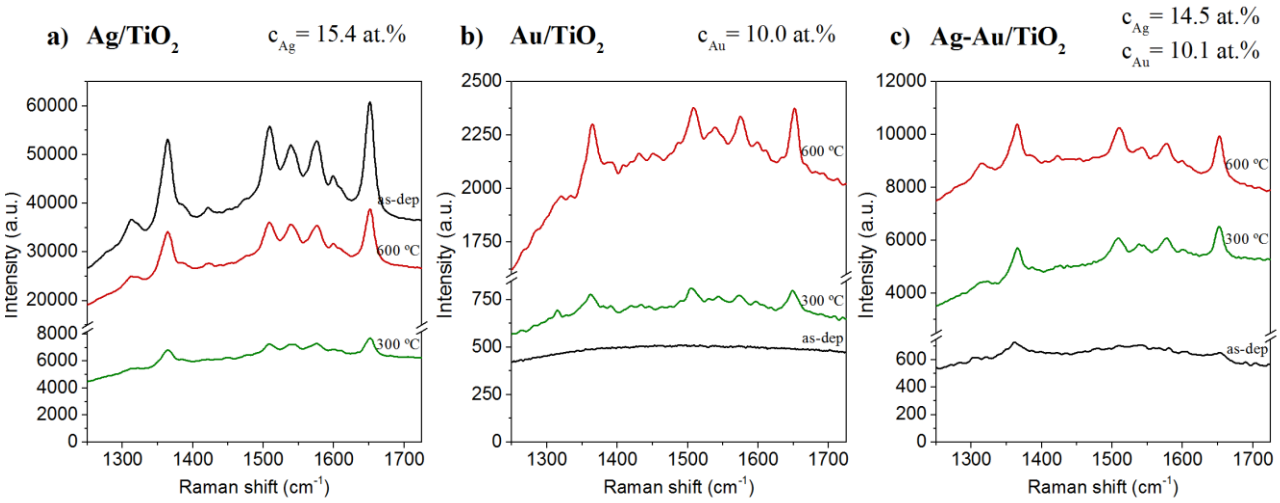

Figure 8 *SERS spectra of the R6G (10^{-4} M solution) adsorbed on (a) Ag/TiO_2, (b) Au/TiO_2 and (c) Ag-Au/TiO_2 thin films.*

According to the results, the use of the Ag/TiO_2, Au/TiO_2 and Ag-Au/TiO_2 samples allowed, in most of the cases, to clearly distinguish the R6G Raman characteristic bands located at 1310 cm^{-1}, 1365 cm^{-1}, 1508 cm^{-1}, 1575 cm^{-1} and 1650 cm^{-1}, associated with the aromatic C-C stretching vibrations of this molecule [56,57]. The Ag/TiO_2 samples are the ones that interacted with the Raman signal of the R6G to give the higher enhancement, while the lowest SERS intensities are observed for the Au/TiO_2 system. Furthermore, the results also showed that the SERS enhancement of the R6G molecules grows significantly with the increase of the annealing temperature for the Au/TiO_2 and Ag-Au/TiO_2 samples, while in the case of the Ag/TiO_2, the as-deposited sample unexpectedly is the one that presents the strongest Raman signal.

The enhancement of the R6G Raman signal is strongly related with the morphological and optical properties of the films, namely the surface roughness, particle size and presence of a LSPR response, which are responsible for an enhancement of the local electromagnetic field and for an efficient charge transfer between the films and the analyte chemical enhancement. Rougher surfaces are expected to provide greater SERS enhancements, not only because they allow a better adsorption of the R6G molecules, but also due to the generation of more hot-spots (i.e. highly localized regions of enhanced EM field) [58]. Furthermore, according to the EM theory, the size of the nanoparticles may be comprised between 5 nm and 100 nm in order to observe the SERS enhancement [59]. Within this order of magnitude, as the size of the nanoparticles increases, their surface area also increases and, consequently, a higher number of R6G molecules might be adsorbed onto them, which therefore results in an improved charge transfer and in an enhanced SERS intensity [60].

The latter may elucidate why the films annealed at higher temperatures, which typically present larger nanoparticles (Figure 5b) and higher surface roughness (Figure 3b and 3c), show, in general, greater enhancements of the R6G Raman signal. It also explains why the Au/TiO_2 films, with smoother surfaces are the ones with the lowest SERS intensities, around one order of magnitude lower than the other systems. However, it does not clarify the behaviour observed in the monometallic nanocomposite Ag/TiO_2 system.

Another important factor that influences the SERS spectra is the existence of a plasmon absorption band, that shall be located between the wavelengths of the laser excitation and the Raman scattered photon for a maximum enhancement of the EM field [61]. It was previously demonstrated that the transmittance of all as-deposited films, as well as of the Ag/TiO_2 samples, revealed an interference-like behavior, while the Au/TiO_2 and Ag-Au/TiO_2 films subjected to heat-treatment presented broad and intense LSPR absorption bands. Although these results may help to explain the increase of the SERS intensity with the heat-treatment for the Au/TiO_2 and Ag-Au/TiO_2 sets of films, they also suggest that, for this kind of systems, the SERS enhancement is mainly attributed to chemical phenomena rather than to the existence of the LSPR effect. This low contribution of the EM

enhancement may probably be attributed to the large width of the LSPR absorption bands and to the fact that the particles responsible for this effect are embedded in the host matrix and, therefore, do not directly interact with the R6G molecules.

Even though the previous discussion might clarify most of the results obtained for the SERS intensity, it fails again to explain the behaviour observed for the as-deposited Ag/TiO_2 sample. In this case, the SEM micrographs (Figure 1a) revealed a microstructure constituted by columns highly separated from one another, which may eventually have increased the effective surface area of the film, creating more adsorption sites for the R6G molecules. Therefore, a stronger interaction with the R6G molecules might have been promoted, which led to a more efficient charge transfer, contributing this way for a higher enhancement of the SERS intensity. In turn, when an annealing treatment is performed, the columnar growth vanishes, and the in-depth porosity induced by it diminishes, thereby affecting the surface area available for SERS activity, leading to a strong decrease of the SERS intensity for the annealed samples comparatively with the as-deposited one. With the increase of the annealing temperature to 600 ºC, large Ag clusters segregated to the top surface of the film, as reported in the SEM analysis (Figure 3a), which promoted a better adsorption of the rhodamine and consequently an increase of its Raman signal comparatively to the samples annealed at 300 ºC.

4. Conclusions

The present work reports the production of Ag/TiO_2, Au/TiO_2, and $Ag\text{-}Au/TiO_2$ nanocomposite thin films deposited by reactive DC magnetron sputtering and followed by an in-air heat-treatment at various temperatures (200 ºC - 700 ºC range). This study intends to showcase the influence of the Ag and Au concentration and of the annealing temperature on the morphology, crystallinity and plasmonic response of the bimetallic $Ag\text{-}Au/TiO_2$ films, taking as refence the corresponding monometallic systems (Ag/TiO_2, Au/TiO_2). In addition, the application to SERS was also accessed using an R6G solution as analyte.

The atomic concentrations of Ag and/or Au in the films was increased by changing the area of metallic pellets placed on the preferential erosion zone of the pure titanium target. Using a reactive atmosphere of $Ar+O_2$ a nearly stoichiometric TiO_2 host matrix was obtained. The morphology of the as-deposited films strongly depended on their chemical composition, varying from a dense and compact structure, as in the case of the Au/TiO_2 films, to a granular voided one, as observed for the Ag/TiO_2 samples. In turn, the as-deposited $Ag\text{-}Au/TiO_2$ films simultaneously comprise dense regions (due to the presence of Au), and granular microstructures (which might be associated to Ag-rich regions) that become more prominent when the metal content increased, indicating an early phase separation between Ag-rich and Au-rich regions throughout the film.

The thermal annealing promoted important microstructural and optical changes in the films, such as the growth of nanoparticles throughout the matrix, segregation of noble metal to the surface under certain conditions, phase crystallization and, in some cases, the appearance of LSPR absorption bands (measured in transmittance mode). Regarding the morphological evolution of Ag/TiO_2 films, initially with columnar voided morphology, the heat-treatment promoted the formation of more disordered and granular microstructures. For the films annealed at higher temperatures (600 - 700 ºC), Ag diffused along their grain boundaries and segregated to the surface, forming large Ag clusters with polyhedral shape or, for higher contents of Ag, dendrite-type fractal structures. On the other hand, for the Au/TiO_2 samples, the dense microstructure is unaltered with the heat-treatment, although the Au nanoparticles that are embedded in the host matrix start to growth and coalesce. In addition, for higher concentrations, Au also segregates to the surface when the films undergo heat-treatment. Regarding the $Ag\text{-}Au/TiO_2$ system, the separation between Ag-rich and Au-rich zones, observed in the as-deposited samples and characterized by the simultaneous presence of dense and granular regions throughout the film, progressively becomes indistinguishable with the increase of the temperature. The thermal annealing promoted the diffusion of the Au and Ag atoms throughout the matrix and the formation of crystalline domains of Ag-Au (in the form of nanoparticles) with fcc structure.

The Ag/TiO_2 films revealed an interference behavior, even with the annealing treatment, and no feature related with LSPR absorption. The most important feature was observed for the film with the highest content of Ag, and annealed at 600 ºC, which revealed a broadband absorption ranging from about 450 nm to 1200 nm in their transmittance and reflectance spectra, associated to the existence of fractal structures on the surface. For the Au/TiO_2 and Ag-Au/TiO_2 films, a strong and large LSPR band are observed when the films are subjected to thermal annealing. In the case of the Ag-Au/TiO_2 samples, the presence of one absorption band, which is narrower and blue-shifted (compared to the Au/TiO_2), confirmed the formation of a bimetallic Ag-Au alloy. This result is particularly important, since it indicates that, in principle, it may be possible to tune the wavelength of the LSPR peak by controlling the concentrations of Ag and Au in the bimetallic nanocomposite Ag-Au/TiO_2 films. This can be performed by "simply" changing the number of Au/Ag pellets placed in the pure target, though the annealing treatment step is always required to promote the growth and coalescence of the nanoparticles. This feature can be useful for several applications such as catalysis, biosensing and optics, where these bimetallic nanoparticles have shown better performance than their monometallic counterparts.

Finally, the SERS response revealed that these films have potential to be used in such application. In particular, the Ag/TiO_2 samples are the ones that better promote the enhancement of the R6G Raman signal even without the heat-treatment. On the other hand, an increase of the annealing temperature also led, in general, to higher SERS enhancements, particularly in the Au-containing systems.

Acknowledgments

This work is financed by National Funds through FCT - Portuguese National Funding Agency for Science, Research and Technology, in the framework of the project PTDC/FIS-NAN/1154/2014 (FCT Projet 9471-RIDTI Reforçar a Investigação, o Desenvolvimento Tecnológico e a Inovação), co-financed by FEDER (POCI-01-0145-FEDER-016902). This research was also sponsored by FCT in the framework of the Strategic Funding UID/FIS/04650/2013. C. G. Ferreira acknowledges CFUM

for the grant CFUM-BI-23/2016- UID/FIS/04650/2013. Joel Borges acknowledges FCT for his Post-Doc Grant SFRH/BPD/117010/2016. Marco S. Rodrigues acknowledges his PhD-Grant from FCT, with reference SFRH/BD/118684/2016.

The first two authors (J. Borges and C.G. Ferreira) contributed equally to this work.

References

[1] Toudert J, Simonot L, Camelio S and Babonneau D 2012 Advanced optical effective medium modeling for a single layer of polydisperse ellipsoidal nanoparticles embedded in a homogeneous dielectric medium: Surface plasmon resonances *Phys Rev B* **86** 45415

[2] Hutter E and Fendler J H 2004 Exploitation of Localized Surface Plasmon Resonance *Adv Mater* **16** 1685–706

[3] Borges J, Kubart T, Kumar S, Leifer K, Rodrigues M S, Duarte N, Martins B, Dias J P, Cavaleiro A and Vaz F 2015 Microstructural evolution of Au/TiO2nanocomposite films: The influence of Au concentration and thermal annealing *Thin Solid Films* **580** 77–88

[4] Borges J, Pereira R M S, Rodrigues M S, Kubart T, Kumar S, Leifer K, Cavaleiro A, Polcar T, Vasilevskiy M I and Vaz F 2016 Broadband Optical Absorption Caused by the Plasmonic Response of Coalesced Au Nanoparticles Embedded in a TiO2 Matrix *J Phys Chem C* **120** 16931–45

[5] Borges J, Rodrigues M S, Kubart T, Kumar S, Leifer K, Evaristo M, Cavaleiro A, Apreutesei M, Pereira R M S, Vasilevskiy M I, Polcar T and Vaz F 2015 Thin films composed of gold nanoparticles dispersed in a dielectric matrix: The influence of the host matrix on the optical and mechanical responses *Thin Solid Films* **596** 8–17

[6] Torrell M, Cunha L, Kabir M R, Cavaleiro A, Vasilevskiy M I and Vaz F 2010 Nanoscale color control of TiO2 films with embedded Au nanoparticles *Mater Lett* **64** 2624–6

[7] Torrell M, Machado P, Cunha L, Figueiredo N M, Oliveira J C, Louro C and Vaz F 2010 Development of new decorative coatings based on gold nanoparticles dispersed in an amorphous TiO2 dielectric matrix *Surf Coatings Technol* **204** 1569–75

[8] Tang L, Kocabas S E, Latif S, Okyay A K, Ly-Gagnon D-S, Saraswat K C and Miller D A B 2008 Nanometre-scale germanium photodetector enhanced by a near-infrared dipole antenna *Nat Photonics* **2** 226–9

[9] Barwicz T, Byun H, Gan F, Holzwarth C W, Popovic M A, Rakich P T, Watts M R, Ippen E P, Kärtner F X, Smith H I, Orcutt J S, Ram R J, Stojanovic V, Olubuyide O O, Hoyt J L, Spector S, Geis M, Grein M, Lyszczarz T and Yoon J U 2007 Silicon photonics for compact, energy-efficient interconnects *J Opt Netw* **6** 63–73

[10] Bingham J M, Anker J N, Kreno L E and Van Duyne R P 2010 Gas Sensing with High-Resolution Localized Surface Plasmon Resonance Spectroscopy *J Am Chem Soc* **132** 17358–

9

[11] Buso D, Post M, Cantalini C, Mulvaney P and Martucci A 2008 Gold Nanoparticle-Doped TiO2 Semiconductor Thin Films: Gas Sensing Properties *Adv Funct Mater* **18** 3843–9

[12] Liu Z, Yu M, Huang S, Liu X, Wang Y, Liu M, Pan P and Liu G 2015 Enhancing refractive index sensing capability with hybrid plasmonic–photonic absorbers *J Mater Chem C* **3** 4222–6

[13] Vaishnav S K, Patel K, Chandraker K, Korram J, Nagwanshi R, Ghosh K K and Satnami M L 2017 Surface plasmon resonance based spectrophotometric determination of medicinally important thiol compounds using unmodified silver nanoparticles *Spectrochim Acta Part A Mol Biomol Spectrosc* **179** 155–62

[14] Endo T, Kerman K, Nagatani N, Hiepa H M, Kim D, Yonezawa Y, Nakano K and Tamiya E 2006 Multiple Label-Free Detection of Antigen-Antibody Reaction Using Localized Surface Plasmon Resonance-Based Core-Shell Structured Nanoparticle Layer Nanochip *Anal Chem* **78** 6465–75

[15] Liu Z Q, Shao H B, Liu G Q, Liu X S, Zhou H Q, Hu Y, Zhang X N, Cai Z J and Gu G 2014 Lambda^3/20000 plasmonic nanocavities with multispectral ultra-narrowband absorption for high-quality sensing *Appl Phys Lett* **104** 81116

[16] O'Neal D P, Hirsch L R, Halas N J, Payne J D and West J L 2004 Photo-thermal tumor ablation in mice using near infrared-absorbing nanoparticles *Cancer Lett* **209** 171–6

[17] Fuertes G, Sánchez-Muñoz O L, Pedrueza E, Abderrafi K, Salgado J and Jiménez E 2011 Switchable bactericidal effects from novel silica-coated silver nanoparticles mediated by light irradiation *Langmuir* **27** 2826–33

[18] Atwater H A and Polman A 2010 Plasmonics for improved photovoltaic devices *Nat Mater* **9** 205–13

[19] Catchpole K R and Polman A 2008 Plasmonic solar cells *Opt Express* **16** 21793–800

[20] Haes A J, Haynes C L, Mcfarland A D, Schatz G C, Van Duyne R P and Zou S 2005 Plasmonic Materials for Surface-Enhanced Sensing and Spectroscopy *MRS Bull* **30** 368–75

[21] Fang Y, Blinn K, Li X, Weng G and Liu M 2013 Strong coupling between Rhodamine 6G and localized surface plasmon resonance of immobile Ag nanoclusters fabricated by direct current sputtering *Appl Phys Lett* **102**

[22] Liu G qiang, Yu M dong, Liu Z qi, Liu X shan, Huang S, Pan P ping, Wang Y, Liu M lin and Gu G 2015 One-process fabrication of metal hierarchical nanostructures with rich

nanogaps for highly-sensitive surface-enhanced Raman scattering *Nanotechnology* **26** 185702

[23] Angelis F De, Das G, Candeloro P, Patrini M, Galli M, Bek A, Lazzarino M, Maksymov I, Liberale C, Andreani L C and Fabrizio E Di 2010 Nanoscale chemical mapping using three-dimensional adiabatic compression of surface plasmon polaritons *Nat Nanotechnol* **5** 67–72

[24] Schuller J A, Taubner T and Brongersma M L 2009 Optical antenna thermal emitters *Nat Photonics* **3** 658–61

[25] Gu X, Qiu T, Zhang W and Chu P K 2011 Light-emitting diodes enhanced by localized surface plasmon resonance *Nanoscale Res Lett* **6** 1–12

[26] O'Connor D and Zayats A V. 2010 Data Storage: The third plasmonic revolution *Nat Nanotechnol* **5** 482–3

[27] Liz-Marzán L M 2006 Tailoring Surface Plasmons through the Morphology and Assembly of Metal Nanoparticles *Langmuir* **22** 32–41

[28] Petryayeva E and Krull U J 2011 Localized surface plasmon resonance: Nanostructures, bioassays and biosensing — A review *Anal Chim Acta* **706** 8–24

[29] Ghodselahi T, Arsalani S and Neishaboorynejad T 2014 Synthesis and biosensor application of Ag@Au bimetallic nanoparticles based on localized surface plasmon resonance *Appl Surf Sci* **301** 230–4

[30] Kumari M M, Jacob J and Philip D 2015 Green synthesis and applications of Au-Ag bimetallic nanoparticles *Spectrochim Acta - Part A Mol Biomol Spectrosc* **137** 185–92

[31] Jacob J, Mukherjee T and Kapoor S 2012 A simple approach for facile synthesis of Ag, anisotropic Au and bimetallic (Ag/Au) nanoparticles using cruciferous vegetable extracts *Mater Sci Eng C* **32** 1827–34

[32] Sebastian S, Linslal C L, Vallbhan C P G, Nampoori V P N, Radhakrishnan P and Kailasnath M 2015 Formation of Au–Ag nanoalloy through Au core/Ag shell intermediate phase by laser ablation *Chem Phys Lett* **628** 25–9

[33] Petrov I, Barna P B, Hultman L and Greene J E 2003 Microstructural evolution during film growth *J Vac Sci Technol A Vacuum, Surfaces, Film* **21** S117–28

[34] Borges J, Rodrigues M S, Lopes C, Costa D, Couto F M, Kubart T, Martins B, Duarte N, Dias J P, Cavaleiro A, Polcar T, Macedo F and Vaz F 2015 Thin films composed of Ag nanoclusters dispersed in TiO2: Influence of composition and thermal annealing on the microstructure and physical responses *Appl Surf Sci* **358** 595–604

[35] Torrell M, Kabir R, Cunha L, Vasilevskiy M I, Vaz F, Cavaleiro A, Alves E and Barradas N P 2011 Tuning of the surface plasmon resonance in TiO2/Au thin films grown by magnetron sputtering: The effect of thermal annealing *J Appl Phys* **109** 74310

[36] Borges J, Rodrigues M S, Lopes C, Costa D, Ferreira A, Pereira R M S, Costa M F, Vasilevskiy M I and Vaz F 2016 Ag fractals formed on top of a porous TiO2 thin film *Phys Status Solidi - Rapid Res Lett* **10** 530–4

[37] Chakravadhanula V S K, Mishra Y K, Kotnur V G, Avasthi D K, Strunskus T, Zaporotchenko V, Fink D, Kienle L and Faupel F 2014 Microstructural and plasmonic modifications in Ag-TiO2 and Au-TiO2 nanocomposites through ion beam irradiation *Beilstein J Nanotechnol* **5** 1419–31

[38] Diop D K, Simonot L, Destouches N, Abadias G, Pailloux F, Guérin P and Babonneau D 2015 Magnetron Sputtering Deposition of Ag/TiO2 Nanocomposite Thin Films for Repeatable and Multicolor Photochromic Applications on Flexible Substrates *Adv Mater Interfaces* **2** 1500134

[39] Samransuksamer B, Horprathum M, Eiamchai P, Patthanasettakul V, Wisitsoraat A, Chananonnawathorn C, Phokharatkul D, Chindaudom P, Jutarosaga T, Rakreungdet W and Dumrongrattana S 2014 Decoration of Gold Nanoparticles on TiO2 Thin Films for Enhanced Response of Ethanol Gas Sensors *Adv Mater Res* **979** 251–4

[40] Naseri N, Sangpour P and Moshfegh A Z 2011 Visible light active Au:TiO2 nanocomposite photoanodes for water splitting: Sol–gel vs. sputtering *Electrochim Acta* **56** 1150–8

[41] Rodrigues M S, Costa D, Domingues R P, Apreutesei M, Pedrosa P, Martin N, Correlo V M, Reis R L, Alves E, Barradas N P, Sampaio P, Borges J and Vaz F 2018 Optimization of nanocomposite Au/TiO2 thin films towards LSPR optical-sensing *Appl Surf Sci* **438** 74–83

[42] Proença M, Borges J, Rodrigues M S, Domingues R P, Dias J P, Trigueiro J, Bundaleski N, Teodoro O M N D and Vaz F 2017 Development of Au/CuO nanoplasmonic thin films for sensing applications *Surf Coatings Technol* **In press**

[43] Pascual-Izarra C, Reis M A and Barradas N P 2006 Simultaneous PIXE and RBS data analysis using Bayesian inference with the DataFurnace code *Nucl Instruments Methods Phys Res B* **249** 780–3

[44] Rodrigues M S, Borges J, Gabor C, Munteanu D, Apreutesei M, Steyer P, Lopes C, Pedrosa P, Alves E, Barradas N P, Cunha L, Martínez-Martínez D and Vaz F 2016 Functional behaviour of TiO2 films doped with noble metals *Surf Eng* **32** 554–61

[45] Smentkowski V S 2000 Trends in sputtering *Prog Surf Sci* **64** 1–58

[46] Depla D, Mahieu S and De Gryse R 2009 Magnetron sputter deposition: Linking discharge voltage with target properties *Thin Solid Films* **517** 2825–39

[47] Rossnagel S 2002 Sputtering and Sputter Deposition *Handbook of Thin-Film Deposition Processes and Techniques* ed K Seshan pp 319–48

[48] Depla D, Mahieu S and Greene J E 2010 Sputter Deposition Processes *Handbook of Deposition Technologies for Films and Coatings* (William Andrew Publishing) pp 253–96

[49] Sangpour P, Akhavan O and Moshfegh A Z 2009 The effect of Au/Ag ratios on surface composition and optical properties of co-sputtered alloy nanoparticles in Au–Ag:SiO2 thin films *J Alloys Compd* **486** 22–8

[50] Borges J, Rodrigues M S, Lopes C, Costa D, Ferreira A, Pereira R M S, Costa M F, Vasilevskiy M I and Vaz F 2016 Ag fractals formed on top of a porous TiO2thin film *Phys Status Solidi - Rapid Res Lett* **10** 530–4

[51] Goodman A M 1978 Optical interference method for the approximate determination of refractive index and thickness of a transparent layer *Appl Opt* **17** 2779–87

[52] Biswas A, Eilers H, Hidden Jr. F, Aktas O C and Kiran C V S 2006 Large broadband visible to infrared plasmonic absorption from Ag nanoparticles with a fractal structure embedded in a Teflon AF® matrix *Appl Phys Lett* **88** 13103

[53] Palik E D 1997 *Handbook of Optical Constants of Solids - Volume I* (Academic Press)

[54] Bass M, Stryland E W, Williams D R and Wolfe W L 2004 *Handbook of Optics* ed M Bass, E W Stryland, D R Williams and W L Wolfe (McGraw-Hill)

[55] Hu Y, Zhang A-Q, Li H-J, Qian D-J and Chen M 2016 Synthesis, Study, and Discrete Dipole Approximation Simulation of Ag-Au Bimetallic Nanostructures *Nanoscale Res Lett* **11** 209

[56] He X N, Gao Y, Mahjouri-Samani M, Black P N, Allen J, Mitchell M, Xiong W, Zhou Y S, Jiang L and Lu Y F 2012 Surface-enhanced Raman spectroscopy using gold-coated horizontally aligned carbon nanotubes *Nanotechnology* **23** 205702

[57] Polavarapu L and Xu Q H 2008 Water-soluble conjugated polymer-induced self-assembly of gold nanoparticles and its application to SERS *Langmuir* **24** 10608–11

[58] Lee C, Robertson C S, Nguyen A H, Kahraman M and Wachsmann-Hogiu S 2015 Thickness of a metallic film, in addition to its roughness, plays a significant role in SERS

activity *Sci Rep* **5** 11644

[59] Moskovits M 2005 Surface-enhanced Raman spectroscopy: A brief retrospective *J Raman Spectrosc* **36** 485–96

[60] Hong S and Li X 2013 Optimal size of gold nanoparticles for surface-enhanced Raman spectroscopy under different conditions *J Nanomater* **2013** 1–8

[61] Merlen A, Gadenne V, Romann J, Chevallier V, Patrone L and Valmalette J C 2009 Surface enhanced Raman spectroscopy of organic molecules deposited on gold sputtered substrates *Nanotechnology* **20** 215705